

# Experimental study of aerosol scattering coefficient pulsations in the near-ground atmospheric layer

I.A. Razenkov, A.P. Rostov, and N.A. Shefer

*Institute of Atmospheric Optics,  
Siberian Branch of the Russian Academy of Sciences, Tomsk*

Received August 5, 1998

Some experimental data are presented on the statistical properties of aerosol content in the near-ground atmospheric layer. The data have been acquired with an *in situ* nephelometer at an acoustical meteorological station. Necessary information on the measurement site is also given in the paper. The estimates obtained based on these measurements show good quality of nephelometric measurements in application to studies of the aerosol fluctuations. The data obtained have been classified in accordance with the Monin–Obukhov similarity theory. Thus constructed classification confirmed that the universal function for the mean aerosol concentration, if it exists, should be analogous to the ones for the air velocity and temperature.

## Introduction

The motion of atmospheric air near the ground surface, from the geophysical-hydrodynamical viewpoint, can be considered as a turbolized wall flow of a fluid in the halfspace.<sup>1</sup> The atmospheric aerosol particles, participating in this flow, are considered as an admixture. The standard Monin–Obukhov theory for near-ground atmospheric layer<sup>1,2</sup> can predict the form of universal laws for mean and statistical parameters of air speed and temperature as well as for any admixture, including the atmospheric aerosol. The admixture, however, must be conservative and passive. The passivity of aerosol, that is, its nonintervention in flow dynamics, is beyond any doubt except dust storm conditions.<sup>7</sup>

On the other hand, the conservative properties of atmospheric aerosol are, seemingly, far from ideal. A conservative admixture must not disappear in the atmosphere. Of course, the aerosol particles are never removed completely from the air; but, nonetheless, aerosol is a dynamic, i.e., variable,<sup>3</sup> atmospheric constituent. Thus the aerosol is dynamically active insofar as it is not ideally conservative, and vice versa. Conditions may occur in the atmosphere favoring constancy of aerosol characteristics in time, but even so, a complex process continuously operates, during which small particles coalesce into intermediate-sized ones, which, in turn, grow to larger ones until deposited on the surface. Therefore, just a few situations can be envisioned when, only to some extent and within a finite time interval, the aerosol can be considered as a conservative admixture.

Being small in size,<sup>12</sup> aerosol particles have an important ability of being almost completely entrained by air flows. Assuming aerosol to be completely conservative, the pulsation of aerosol concentration would be entirely determined by fluctuations of the turbulent flow speed.<sup>10</sup> Then, the Monin–Obukhov similarity theory would be strictly valid for an

atmospheric aerosol admixture. The Monin–Obukhov theory describes the state of near-ground air layer and makes it possible to systematize the observational data on the mean values and pulsations. Therefore, the experimental study of air speed pulsations can help a better understanding of (1) to what extent the of atmospheric aerosol can be treated as a conservative admixture; and (2) what are the other variables, besides air speed fluctuations, that may influence the particle concentration in a turbulent flow?

By aerosol concentration we mean the concentration of only those particles that make up the main fraction of the aerosol mass. Note also that the term “total concentration of particles” is physically uncertain for it depends on the instrument’s resolution. On the other hand, at any time the atmosphere contains many finely dispersed particles less than 0.01  $\mu\text{m}$  in radius, with negligibly small mass, that contribute only insignificantly to light scattering. In what follows, the particle concentration will be meant as the concentration of aerosol particles with the radii equal to or larger than 0.1  $\mu\text{m}$ .

As known, the turbulence is characterized by random displacements of some air parcels relative to others; and as such, the effect of turbulence on aerosol concentration is to regulate, in a given air volume, the number and, hence, the total mass (content) of particles in accordance with hydrodynamics laws. By “aerosol content” we will mean the volume (mass) of aerosol substance per unit air volume.

Through the dynamic impact on aerosols, the turbulent flow governs the formation of altitude profiles of the mean particle concentration, variance of fluctuations, and other statistical characteristics of the aerosol content in the atmosphere. Obviously, the profile shape will depend on the state of atmospheric turbulence and particle formation rate at the underlying surface.

The primary goal of this study was to concentrate on the experimental study of the variance of

fluctuations and turbulence-generated aerosol mass fluxes by means of the Monin–Obukhov similarity theory for thermally stratified near-ground air layer. This study was also aimed at investigation of the behavior of transformation coefficient of aerosol scattering phase function as a function of hydrostatic stability parameter. Besides, a part of the effort was spent to validate the use of optical method adopted in this study.

Earlier, by studying the statistical properties of aerosol formations, we obtained the frequency spectrum of the power of aerosol coefficient fluctuations,<sup>10</sup> and estimated characteristic spatial scales of aerosol inhomogeneities and their typical lifetime.<sup>12</sup> Based on lidar data, we revealed and documented substantial differences between behaviors of turbulent heat and aerosol mass fluxes for different states of near-ground atmospheric layer.<sup>13</sup> Those studies addressed either applied problems, or documented some experimental facts. We note that the present literature contains little experimental data on fluctuations of concentration of atmospheric aerosol as an admixture of turbulent air flows, probably because of technical problems, not overcome until recently.

Let us discuss the physical aspects of the problem, dealing with the random properties of gas-aerosol atmospheric admixture, and specific ways of its solution. Experimental study of atmospheric aerosol is difficult because of (1) complex nature of this constituent (wide particle size spectrum, polydisperse structure, chemical composition, etc.) and (2) great variety of processes the aerosol is involved in (coagulation, sedimentation, etc.).

The reasons why the optical method has been chosen for these studies have to be explained. The optical (nephelometric) method of determining aerosol content from measurements of coefficients of directional scattering is characterized by high sensitivity and is very fast.<sup>9</sup> Nephelometric measurements can be made *in situ* with high sampling rate, which is especially important when random processes are studied.<sup>8</sup> Below we will consider in a more detail the optical method of determining aerosol content in the air volume studied.

We note that fluctuations of air humidity, as well as other atmospheric gaseous constituents, had little influence on measurements of fluctuating aerosol scattering coefficient, since absorption bands at the wavelength the nephelometer operates at (0.85  $\mu\text{m}$ ) are rather weak.

## Method

Usability of the method chosen here to measure aerosol particle concentration will become clear after answering the following questions:

1) What particles contribute most to the signal caused by light scattering at 45° angle, at which the nephelometer measurements<sup>15</sup> are performed at the wavelength  $\lambda = 0.85 \mu\text{m}$ ?

2) Which fraction of aerosol particles ensemble is responsible for this signal?

These parameters, the wavelength and the scattering angle, have been chosen here because these are the working parameters of a nephelometer based on a high-power silicon diode emitting in the IR; this is a reliable and sensitive nephelometer, for *in situ* measurements, being technically most easily manufactured. Physically, the scattering angles near 45° are important because particles of all sizes contribute nearly equally to the scattering along this direction. In other words, directional scattering coefficient, calculated for 45°, correlates best of all with the total scattering coefficient.

As known, measured particle size spectra are multimode because atmospheric aerosol originates from many sources.<sup>3</sup> This motivated the separation of particle diameter range into three main aerosol fractions (modes): fine-disperse (0.01–0.1  $\mu\text{m}$ ), submicron (0.1–1  $\mu\text{m}$ ), and coarse-disperse fraction (> 1  $\mu\text{m}$ ). Particles of the fine fraction (photochemical or transient fraction) form as a result of synthesis of particulate matter from atmospheric gases. The particles of this fraction rapidly coagulate into submicron particles, with almost no further coagulation.<sup>3</sup> In turn, particles of the coarse fraction are formed in the process of soil erosion and, as such, are subject to strong dynamic variations.

Submicron aerosol is easily entrained by air flows, it can be transported at long distances, and has low sedimentation (deposition) rate, quite uniform spatial distribution, and rather weak dependence on how other fractions evolve.<sup>3</sup> That is why the particles of this size are most frequently chosen as a subject for research when developing instrumentation for studies.

In the absence of universally accepted term, different authors refer to aerosol fraction, corresponding to size range from 0.1 to 1  $\mu\text{m}$ , as submicron, condensation-mode, accumulation-mode, or optical mode.

The disperse composition of atmospheric haze can be considered as a structure comprising three relatively independent subsystems (fractions); therefore, to fit the particle volume size distribution, Ref. 3 proposed the second-order regression curve

$$\frac{dV_i}{dr} = \frac{4}{3} \pi r^3 \frac{dN_i}{dr} = AM_i \exp \left[ -b_i \left( \ln \frac{r}{r_{V_i}} \right)^2 \right], \quad (1)$$

where index  $i$  is equal to 1 for fine fraction, 2 for the submicron fraction, and 3 for the coarse aerosol fraction;  $V_i$  is the volume occupied by the  $i$ th aerosol fraction;  $r$  is the particle radius;  $N_i$  is the particle number density in the  $i$ th fraction;  $r_{V_i}$  is the mean “volumeB radius of particles of the  $i$ th fraction;  $M_i$  is the weighting factor of the  $i$ th fraction;  $A$  is a constant; and  $b_i$  is the parameter related to the standard deviation  $\sigma_{V_i}$  as

$$b_i = -\frac{1}{2} (\ln \sigma_{V_i})^2. \quad (2)$$

To better understand which particles contribute most to the scattered signal at infrared wavelengths, let us refer to Ref. 4, which defined, based on Mie theory, and calculated a criterion quantifying the optical effectiveness of different aerosol fractions:

$$\beta [\lambda, m, f(r), \theta] = \frac{\int_0^r K [\lambda, m, f(r), \theta] f(r) dr}{\int_0^\infty K [\lambda, m, f(r), \theta] f(r) dr}, \quad (3)$$

where  $K [\lambda, m, f(r), \theta]$  is the coefficient of optical interaction for the particle with size  $r$  and refractive index  $m(\lambda)$  at the wavelength  $\lambda$  and scattering angle  $\theta$  (coefficient of directional interaction). Functional (3) determines the relative cumulative contribution of particles with radii  $r \in [0, r]$ , having the size spectrum determined by the function  $f(r)$ , to the integrated directional scattering coefficient.

Figure 1 shows three size-distribution functions for particle's volume calculated by formula (1) for different air turbidity in the presence of large particles ( $M_3 = 0; 0.06; 0.5$ ). For size spectra shown in Fig. 1 (curves 2 and 3), Ref. 3 calculated functional (3) for  $\lambda = 0.7 \mu\text{m}$ . Figure 2 shows the dependences of the functional (3) (curves 2 and 3) on particle radius. The weighting factor  $M_3 = 0.06$  corresponds to weak turbidity, while  $M_3 = 0.5$  to a strong one. From Fig. 2 it follows that at  $\lambda = 0.7 \mu\text{m}$  the major (more than 80%) contribution to the scattered signal comes from particles having radii from 0.1 to 1  $\mu\text{m}$ . The integrated

particle size-distribution function  $p(r) = \int_{0.1}^r f(r) dr$  is presented in Fig. 2 (curve 1).

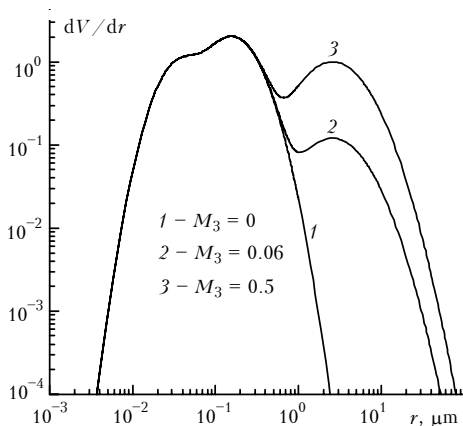


Fig. 1. Model volume size-distribution function of aerosol particles under conditions of no large particles (curve 1) present and weak (curve 2) and strong (curve 3) atmospheric turbidity.

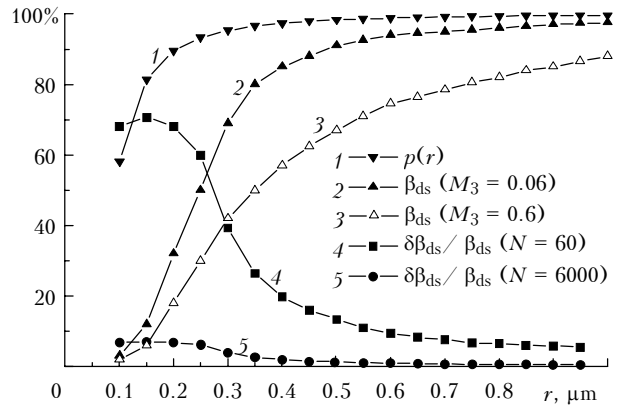


Fig. 2. Cumulative (over particle radius) contribution of aerosol fractions to the scattering coefficient at the wavelength of 0.7  $\mu\text{m}$  for weak (curve 2) and strong (curve 3) atmospheric turbidity, together with the integrated size-distribution function (curve 1) and integrated statistical error of determining scattering coefficient for  $N = 60$  (curve 4) and  $N = 6000$  (curve 5).

To estimate the fractional content of submicron aerosol, the integrated particle volume of the fraction  $i$  is calculated as<sup>3</sup>:

$$V_i = r_{V_i} \sqrt{\pi/b_i} AM_i \exp(1/4b_i). \quad (4)$$

Correspondingly, the particle number density in the fraction  $i$  is calculated as

$$N_i = \frac{3}{4\pi} \frac{1}{r_{V_i}^2} \sqrt{\frac{\pi}{b_i}} AM_i \exp\left(\frac{1}{b_i}\right). \quad (5)$$

Here we will use mean  $r_{V_i}$  and  $\sigma_{V_i}$  values corresponding to continental aerosol of the planetary boundary layer from Ref. 3 that are reproduced in Table 1.

Table 1

| Aerosol fractions |                |           |                |           |                |
|-------------------|----------------|-----------|----------------|-----------|----------------|
| fine-disperse     |                | submicron |                | coarse    |                |
| $r_{V_1}$         | $\sigma_{V_1}$ | $r_{V_2}$ | $\sigma_{V_2}$ | $r_{V_3}$ | $\sigma_{V_3}$ |
| 0.038             | 1.72           | 0.16      | 1.84           | 2.57      | 2.22           |

Using expressions (4) and (5) and the values from Table 1, we can calculate the relative volume of submicron aerosol particles as

$$\beta_V = V_2 / (V_1 + V_2 + V_3) \times 100\%. \quad (6)$$

Table 2 presents the particle number density  $N_i$  for all fractions, relative contribution of submicron fraction to the directional scattering (at angle 40°), coefficient  $\beta_{ds}$  for the wavelength  $\lambda = 0.7 \mu\text{m}$ , and relative volume  $\beta_V$  of the submicron aerosol fraction. Calculations are made for the number density  $N(r > 0.1 \mu\text{m}) = 60 \text{ cm}^{-3}$  (see Ref. 3).

Table 2

| No. | $M_1$ | $M_2$ | $M_3$ | $N_1, \text{cm}^{-3}$ | $N_2, \text{cm}^{-3}$ | $N_3, \text{cm}^{-3}$ | $\beta_{\text{ds}}, \%$ | $\beta_V, \%$ |
|-----|-------|-------|-------|-----------------------|-----------------------|-----------------------|-------------------------|---------------|
| 1   | 0     | 1     | 0     | 0                     | 60                    | 0                     | 100                     | 100           |
| 2   | 0.5   | 1     | 0     | 405                   | 60                    | 0                     | 97                      | 91            |
| 3   | 0.5   | 1     | 0.06  | 405                   | 60                    | 0.031                 | 94                      | 39            |
| 4   | 0.5   | 1     | 0.5   | 405                   | 60                    | 0.258                 | 86                      | 8             |

The values in the first line of Table 2 are for the case with no small and large particles present ( $M_1 = M_3 = 0$ ), the second line is for the case with no large particles only ( $M_3 = 0$ ), the third line is for weak-turbidity conditions ( $M_3 = 0.06$ ), and the fourth line is for strong-turbidity conditions ( $M_3 = 0.5$ ). As is evident from Table 2, the relative weight of submicron particles is about 40% under conditions of weak turbidity ( $M_3 = 0.06$ ) and is only 8% under strong-turbidity regime. Occasionally, a cubic centimeter of air may contain no large-sized particles since  $N_3 < 1 \text{ cm}^{-3}$ . Assuming the scattering volume of an actual nephelometer to be  $100 \text{ cm}^3$ , we can readily calculate that there would be about 40000 small, optically inactive particles, 6000 optically active particles, and about 3 large particles when  $M_3 = 0.06$  and 26 large particles when  $M_3 = 0.5$ . It should be noted, however, that the weight of three large particles will be equal to or even larger than the weight of 6000 submicron particles.

Hydrodynamic considerations dictate that the medium ought to be continuous<sup>1</sup>; for which, obviously, the number of particles in it must be sufficiently large.

Let us estimate the error (uncertainty) of determining the number of particles in the volume under study. First of all, these particles are few in number that may be counted, at any time; so we assume that fluctuations of the number of particles are described by the Poisson law:

$$P(N, \langle N \rangle) = \langle N \rangle^N / N! \exp(-\langle N \rangle), \quad (7)$$

where  $P$  is the probability of detecting  $N$  particles, when the mean number of particles in a given measurement series is  $\langle N \rangle$ .

For statistical distribution (7), the uncertainty  $\delta N$  of determining the mean number of particles  $\langle N \rangle$  in a set of  $m$  measurements can be approximately expressed as

$$\delta V^2 \approx \langle N \rangle / m. \quad (8)$$

This formula implies that the error of estimating the number of aerosol particles scales as the inverse square root of the number of measurements.

Since the nephelometer output signal is proportional to the coefficient  $\beta_{\text{ds}}$  and, correspondingly, to the value of  $\beta \equiv \beta[\lambda, m, f(r), \theta]$  defined by Eq. (3) at fixed parameters, the error of estimating  $\beta_{\text{ds}} \sim \beta$  can be evaluated, if (3) is differentiable with respect to  $p(r)$ , as

$$\delta \beta = \frac{\partial \beta}{\partial p} \frac{\partial p}{\partial N} \delta N. \quad (9)$$

Equation (9), with account of Eq. (8), was used to estimate the error of calculating  $\beta_{\text{ds}}$  curves shown in Fig. 2; the results are presented in Fig. 3 (curve 4 is for  $N = 60$ ; curve 5 is for  $N = 6000$ , and curve 2 is same as in Fig. 2, with  $M_3 = 0.06$ ). These curves illustrate the statistical error of determining the coefficient of scattering at  $40^\circ$  angle for particles with radii  $r \in [0, r]$ . We see that the error of  $\beta_{\text{ds}}$  determination is about 6% for  $1 \text{ cm}^3$  ( $N = 60$ ) sampled volume of air, and less than 1% for  $100 \text{ cm}^3$  ( $N = 6000$ ) volume. Making  $m$  such measurements and averaging will lead to  $\sqrt{m}$  times less error.

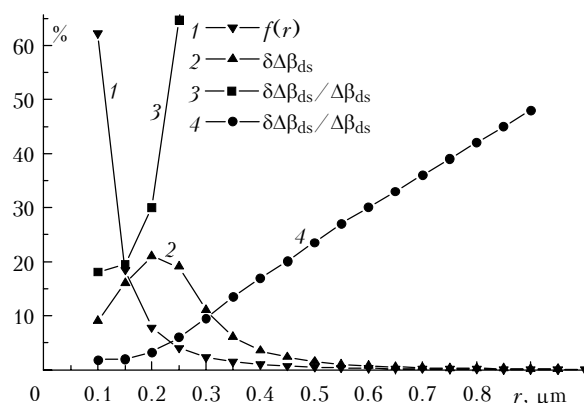


Fig. 3. Contribution of aerosol particles of different radii to the scattering coefficient at the wavelength of  $0.7 \mu\text{m}$  for weak turbidity (curve 2), together with size-distribution function (curve 1) and statistical error of determining scattering coefficient for  $N = 60$  (curve 3) and  $N = 6000$  (curve 4).

If particles in each size range could be counted separately, the inaccuracy of their measurements could also be calculated by formula analogous to Eq. (9), but now with the difference  $\Delta\beta$  between neighboring  $\beta$  values used instead of  $\beta$ , and with the function  $f(r)$  used instead of  $p(r)$ . An example of such calculation, with  $N = 60$  (curve 3) and  $N = 6000$  (curve 4), is presented in Fig. 3. As seen, the error of  $\Delta\beta$  evaluation (curve 2) rapidly increases with growing particle radius. Here, curve 1 shows the distribution function  $f(r)$ .

The above analysis has shown that the optical method is quite applicable to measurements of aerosol content in a small volume under weak turbidity conditions ( $M_3 = 0.06$ ). Moreover, when aerosol content is measured in the turbulent flow carrying submicron particles only, the nephelometer operation may appear to be almost ideal.

## Theory

Vertical turbulent flows play an important part in such inhomogeneous turbulent flows, as the near-ground atmospheric layer. Friction between moving air and Earth's surface gives rise to the gradient of the modulus of wind velocity and to a momentum flux. The daytime (nighttime) surface warming (cooling) produces lapse rate of atmospheric temperature and the corresponding ascending (descending) heat fluxes. The vertical turbulent fluxes of momentum and heat,  $\tau$  and  $H_v$ , as well as the vertical turbulent aerosol mass fluxes  $H_a$  are determined easier and more accurately by direct methods, from pulsation observations and averaging of the relevant products

$$\tau = -\rho \langle u' w' \rangle, \quad (10)$$

$$H_v = c_p \rho \langle w' T' \rangle, \quad (11)$$

where  $\rho$  is the air density;  $c_p$  is the heat capacity at constant pressure;  $u'$  is the pulsation component of the longitudinal wind velocity;  $w'$  is the pulsation of the vertical velocity; and  $T'$  is the pulsation component of temperature.

Suppose that we can experimentally measure some quantity  $A$ , proportional to the aerosol content  $\rho_a$ ; and let us introduce the proportionality constant that may have the dimensionality of

$$A = C_1 \rho_a. \quad (12)$$

Let  $A$  denote, in the general case, the directional scattering coefficient proportional to the particle number density. We note that the presence of  $C_1$  will have no consequences on our inference. By analogy with Eq. (11), we will write an expression for the turbulent flux of aerosol scattering coefficient in the form

$$H_a = \rho \langle w' A' \rangle, \quad (13)$$

where  $A'$  is the pulsation component of the aerosol scattering coefficient.

The phrase "turbulent flux of scattering coefficient" is physically meaningless, so we will use the term "turbulent aerosol mass flux," while always having in mind that the scattering coefficient is proportional to the aerosol content. The turbulent flux of aerosol mass occurs in the atmosphere due to the presence of vertical gradient of the aerosol density: aerosol concentration generally decreases with height above the surface representing the aerosol source.

The velocity and temperature gradients, in a combination, can be used to quantify, in terms of momentum and heat fluxes, the thermodynamic state of near-ground atmospheric layer; and this can be done only through calculation of scales of velocity (friction velocity  $u_*$ ), temperature ( $T_*$ ), and length (Monin-Obukhov scale  $L_*$ ).

It should be stressed that there are two different definitions for the "near-ground atmospheric layer." In the geophysical hydrodynamics sense,<sup>2</sup> it is the layer adjacent to the surface, with the depth defined by requirement that the momentum and heat fluxes and mass fluxes of any admixture vary by no more than 20% within it; so its thickness typically ranges from 10 (at night) to 100 m (during daytime), depending on meteorological conditions. Alternatively, the aerosol near-ground layer is considered to extend from the surface to the altitude of 2–4 km. Here, we assume the first alternative, that is a 50-m-thick air layer adjacent to the surface.

Usually, the initial experimental data on the turbulent near-ground layer are interpreted and systematized using Monin-Obukhov similarity theory,<sup>3</sup> which, like any other similarity theory, aims at establishing the relationships between different dimensionless variables. Typically, such relationships are universal.

In principle, the Monin-Obukhov theory can be used to estimate the scale, for measurements in dimensionless units, of any atmospheric conservative passive admixture, and to classify the obtained results (such as vertical profiles, variances, and turbulent fluxes, among others).

The similarity theory rests on the hypothesis, first introduced by Monin and Obukhov in 1953, which states that, in the region of developed turbulence in the inertial range of wavenumbers, the turbulent regime does not depend on molecular constants, and that, at heights exceeding the mean size of surface roughness, the surface properties have no significant effect on the vertical variations of statistical characteristics of hydrodynamic fields.<sup>1</sup> Thus the altitude dependences of velocity and temperature fields are determined by the parameters

$$u_* = \sqrt{-\langle u' w' \rangle}, \quad (14)$$

$$\beta = g/T, \quad (15)$$

$$T_* = -\langle w' T' \rangle / (\kappa u_*), \quad (16)$$

where  $\beta$  is buoyancy;  $g$  is the acceleration of gravity;  $T$  is the temperature of the medium in Kelvin; and  $\kappa$  is the Karman constant equal to 0.4.

These quantities can be combined to yield the scale of Monin-Obukhov length

$$L_* = u_*^2 / (\kappa^2 \beta T_*). \quad (17)$$

According to the above mentioned hypothesis, the dimensionless velocity and temperature, measured on scales  $u_*$  and  $T_*$ , must be universal functions of dimensionless height

$$\xi = z/L_*, \quad (18)$$

which is the main local criterion of hydrostatic stability (similarity principle).<sup>1</sup>

By analogy with Eqs. (14) and (16), we can define the parameter-scale  $A^*$ , in units similar to that of  $A$ ,

$$A_* = - \langle w' A' \rangle / (\kappa u_*), \quad (19)$$

where  $A'$  is the pulsation component of the parameter  $A$  which, like the velocity and temperature, can be represented as a sum of the mean  $\langle A \rangle$  and its random deviation  $A'$  from zero mean,  $A = \langle A \rangle + A'$ . Note that, as for  $A_*$ , for  $\rho_a$  we can define a scale  $\rho_{a*}$ , with  $A_*$  and  $\rho_{a*}$  scales different to a constant factor  $C_1$ . Unfortunately, the  $C_1$  determination is technically difficult, and it is not attempted here.

According to the similarity principle outlined above, the dimensionless vertical gradients of the mean values of wind velocity  $\langle u \rangle$  and an arbitrary passive admixture  $\langle A \rangle$  can be written as

$$\frac{\partial \langle u \rangle}{\partial z} = \frac{u_*}{\kappa L_*} \frac{1}{\xi} \varphi_u(\xi); \quad (20)$$

$$\frac{\partial \langle A \rangle}{\partial z} = \frac{A_*}{L_*} \frac{1}{\xi} \varphi_A(\xi), \quad (21)$$

where  $\varphi_u(\xi)$  and  $\varphi_A(\xi)$  are universal functions of the argument  $\xi$ .

For certainty, by  $A$  we mean the aerosol content. Upon integrating, (20) and (21) take the form

$$\langle u(z) \rangle = (u_* / \kappa) f_u(\xi) + C_u; \quad (22)$$

$$\langle A(z) \rangle = A_* f_A(\xi) + C_A, \quad (23)$$

where  $f_u(\xi)$  and  $f_A(\xi)$  are the integrands of  $\varphi_u(\xi)$  and  $\varphi_A(\xi)$ .

The similarity theory predicts the existence of universal profiles of  $f_u(\xi)$  and  $f_A(\xi)$  and other admixtures. Generally speaking, the functions  $f_u(\xi)$  and  $f_A(\xi)$ , as well as others of that type, have very similar shapes<sup>1</sup>; but their detailed view can be determined by experiment.

Note that when a universal profile of the average  $f_\alpha(\xi)$  is determined (with  $\alpha$  standing for velocity, temperature, or some other admixture), the uncertainty of specifying the "reference point B for the function  $f_\alpha(\xi)$ " can be eliminated by adding the extra term  $-f_\alpha(\pm L_*/n)$ , where  $n$  is typically set to 2, 10, or 20. The Refs. 1 and 2 extensively studied the universal profiles of  $f_\alpha(\xi) - f_\alpha(|L_*/n)$  for the wind velocity, temperature, and humidity.

## Instrumentation

A two-angle, open-cell nephelometer, especially designed to study the statistical properties of aerosol concentration, has been described in Ref. 15. It is assembled based on light-emitting and photo-diodes, having maximum response to radiation with the

wavelength  $\lambda = 0.85 \mu\text{m}$  at the viewing angles 45 and 170°. The second channel, of sighting at 170°, is used to monitor changes in aerosol microstructure, i.e., in aerosol scattering phase function.

Note that, while not absolutely calibrated, the nephelometer response was checked every time using strongly attenuating neutral density filters and an opaque screen placed in the same position at the center of the working volume of the nephelometer. This ensured relative nephelometer calibration during the measurements. During two years of its operation, nephelometer little changed its performance characteristics and required no additional adjustments.

In the measurements we used nephelometer together with an ultrasonic acoustic meteorological station<sup>16</sup> that allowed us to measure *in situ* three components of wind velocity and ambient air temperature. The meteorological station and nephelometer were equipped with the microcontrollers and modems, the former for data storage, and the latter for data transmission to the central computer located in the operator's cabin at a considerable distance from the measurement site. The instrumentation (sensors) were installed on the mast in the field and were operated continuously for a long time; but in rain it was dismantled.

## Experiment

The field measurements were performed at the field measurement site of the Institute of Atmospheric Optic (IAO) near city of Tomsk. The measurement is an even field with oats crop. The meteorological station and the nephelometer were located on the meteorological mast at a height of 5 m. The meteorological station measured three components of wind velocity and air temperature, while the nephelometer measured scattering coefficient at the scattering angles of 45 and 170°.

The instruments were operated synchronously at a rate of 2 Hz. During one measurement cycle (17 min, 2048 counts), the measured data were fed into a computer and recorded on its hard disc as a file. Then, this procedure was repeated again, potentially many times, unless rain occurred.

The experiment was conducted in summer and fall seasons of 1996 and 1997, during that period more than 700 17-min-long measurement series have been acquired. In summer of 1996, heavy rains washed out aerosol particles from the atmosphere; for this reason, most of the data had low signal-to-noise ratio and were excluded from the consideration.

Each of the 17-min measurement cycle was processed separately. The processing included data correction with account of wind direction (through determining transverse and longitudinal wind velocity components), removal of false measurements (by applying Chebyshev inequality), averaging, detrending, and calculation of variance. Detrending,

in the form of high-frequency polynomial filtering,<sup>8</sup> was used to eliminate nonstationarity of the processes studied.

Next, the data were subjected to Fourier analysis by applying fast Fourier transform.<sup>8</sup> The result was auto- and cross-spectra of power fluctuations of signals and the corresponding correlation functions.

Turbulent momentum, heat, and particulate mass fluxes,  $\langle u' w' \rangle$ ,  $\langle w' T' \rangle$ , and  $\langle w' A' \rangle$ , were determined by taking averages of the appropriate products; and then the scales  $u_*$ ,  $T_*$ ,  $L_*$ ,  $A_*$ , and the parameter of hydrostatic stability  $\xi$  were estimated by formulas (14), (16), (17), (18), and (19).

No universal profiles of the mean meteorological parameters and aerosol concentration, as defined by Eqs. (22) and (23), were determined because of unavailability of appropriate altitude-stratified measurements. Nevertheless, we calculated the following functions:

$$\frac{\langle u \rangle}{u_*} = \frac{f_u(\xi)}{\kappa} + C_u; \tag{24}$$

$$\langle A \rangle / A_* = f_A(\xi) + C_A, \tag{25}$$

which coincide with the mean universal profiles accurate to a constant.

### Results

It is necessary to describe the terrain relief of the measurement site. It is a field extended in the south-north direction, 3 km by 1 km in size. The measurement site was located at the field center, approximately 100 m to the east of a small village on the same field.

Figure 4a is a polar diagram showing absolute values of wind velocity for each 17-min-long measurement cycle made in 1996 and 1997. Wind direction was predominately from south and south-west, consistent with wind rose for Tomsk.

The surface roughness of the measurement site territory was quantified in terms of the friction drag coefficient

$$c_d = \frac{\tau}{\frac{1}{2} \rho \langle u \rangle^2} = 2 \left( \frac{u_*}{\langle u \rangle} \right)^2. \tag{26}$$

The coefficient  $c_d$  characterizes the balance between the mechanical turbulence energy and the kinetic energy flux. The greater the surface roughness, the larger the  $c_d$  value. This dependence is illustrated by the diagram in Fig. 4b, where the maximum  $c_d$  value corresponds to the wind from the west, i.e., the direction from the village.

Another frequently used surface characteristic is the dynamic roughness  $z_0$ , physically equivalent to the boundary condition on the underlying surface where the wind is, on the average, zero. The  $z_0$  value can be calculated when indifferent (neutral) thermal

stratification (with  $\xi = 0$ ) is established in the near-ground layer, with the wind velocity varying logarithmically with altitude.<sup>1</sup>

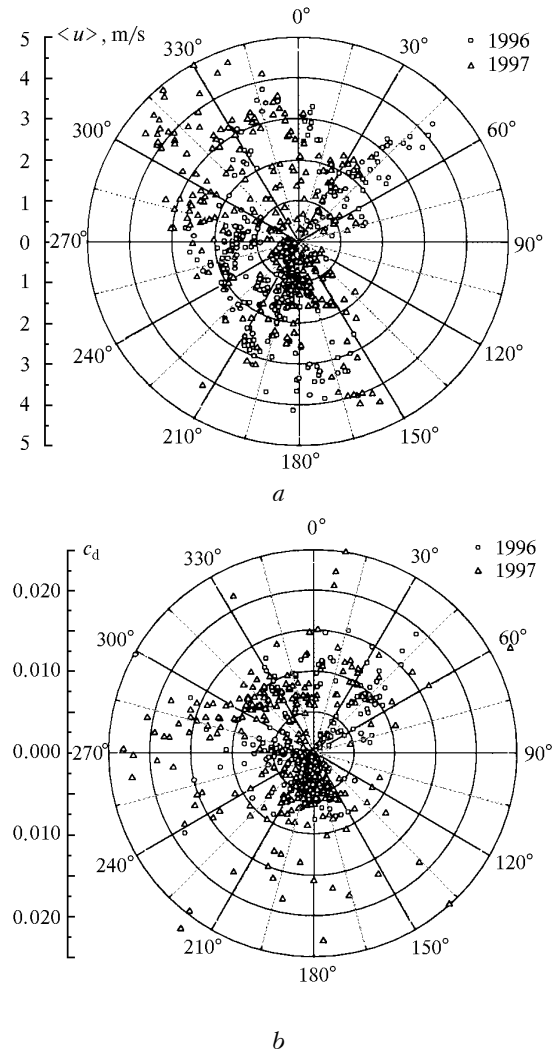
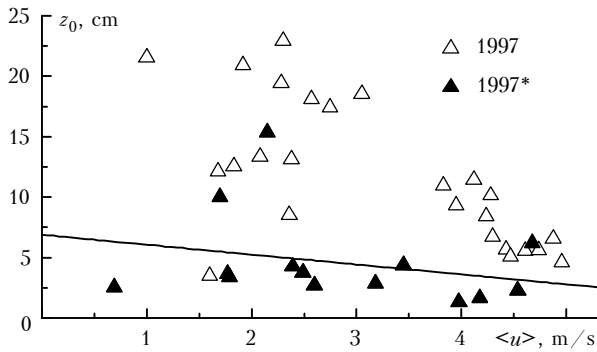


Fig. 4. Polar diagrams of the mean wind speed (a) and friction drag coefficient (b) based on measurement data obtained in 1996 and 1997 at the IAO measurement site.

Figure 5 shows, for conditions considered, as usually neutral ( $|\xi| \leq 0.03$ ) in 1997,  $z_0$  values for all wind directions and for directions from south to north or opposite. As seen, the  $z_0$  values are less in the second than in the first case and decrease from 7 cm to 3 cm as wind speed increases from 1 to 5 m/s. The explanation is that the stronger the wind, the greater its bending-down effect on the grass, and, hence, the less the surface roughness. This finding well agrees with the results of other authors,<sup>2</sup> obtained for 50 to 70 cm-tall grass.

Results presented here and elsewhere<sup>14,17</sup> indicate that, in a wide frequency interval, the spectrum of fluctuations of scattering coefficient in the near-ground layer follows the Kolmogorov's  $-5/3$  power law. This very important fact suggests that the submicron particles are completely entrained and that

they are, to a considerable degree, conservative and passive during the observations.



**Fig. 5.** Surface roughness of the field for all wind directions (open triangles) and directions along the long field axis (closed triangles) measured in 1997.

Here we would like to note that the deployed instrumentation frequently failed to respond adequately to the rapidly changing ambient conditions what represents a practical limitation to the study of the medium fluctuations in terms of power spectra and other statistical characteristics. This inadequacy sometimes may lead to deviation from the  $-5/3$  power law due to too low signal relative to the noise, with the signal-to-noise ratio near or below unity. This circumstance is illustrated by Fig. 6, showing the spectra of fluctuations of longitudinal component of wind velocity (Fig. 6a) and the spectra of aerosol fluctuations (Fig. 6b) for the cases of neutral ( $\xi = 0$ ) and unstable ( $\xi = -0.56$ ) stratification. For wind velocity, the signal-to-noise ratio exceeded 8 in both cases; whereas for aerosol scattering, its value was 2.5 in the first case and only 0.1 in the second one. Correspondingly, the spectrum in Fig. 6b follows the Kolmogorov's power law down to the frequency of 0.2 Hz in the first case, and exhibited white noise everywhere in the second case. Here, the value of signal-to-noise ratio was estimated from the jump of the autocorrelation function at the zero time lag.<sup>18</sup> Such a strong variability of signal-to-noise ratio for scattering coefficient, arising due to strong dependence of the amplitude of scattering coefficient fluctuations on the state of the near-ground layer, explain why the measurements of the scattering coefficient fluctuations are so difficult.

On the whole, the total data set for 1996 and 1997 was characterized by rather low signal-to-noise ratio for the scattering coefficient; providing no chance to study the variance of fluctuations of the scattering coefficient, as well as other characteristics, in full extent. Uncorrelated noise has little influence on the estimates of vertical aerosol flux  $H_a$  and scale  $A_*$  because in this case different noise components cancel each other.

Having this fact in mind, we calculated the ratios of horizontal to vertical fluxes for temperature (Fig. 7a) and aerosol (Fig. 7b). By analogy to vertical turbulent fluxes,

the horizontal fluxes were calculated by formulas (11) and (13), but with longitudinal wind component  $u'$  used instead of vertical pulsation component  $w'$  therein. From simple physical considerations<sup>1</sup> it follows that this ratio is always negative. In Fig. 7, the curve shown by solid line is calculated based on Monin–Ellison theory.<sup>2</sup> As seen, the heat and aerosol show similar behavior in this case. The data on heat obtained do not contradict the findings of other authors.<sup>2</sup> From Fig. 7 it follows that, as the instability grows in magnitude, the vertical fluxes increase until comparable to the horizontal ones.

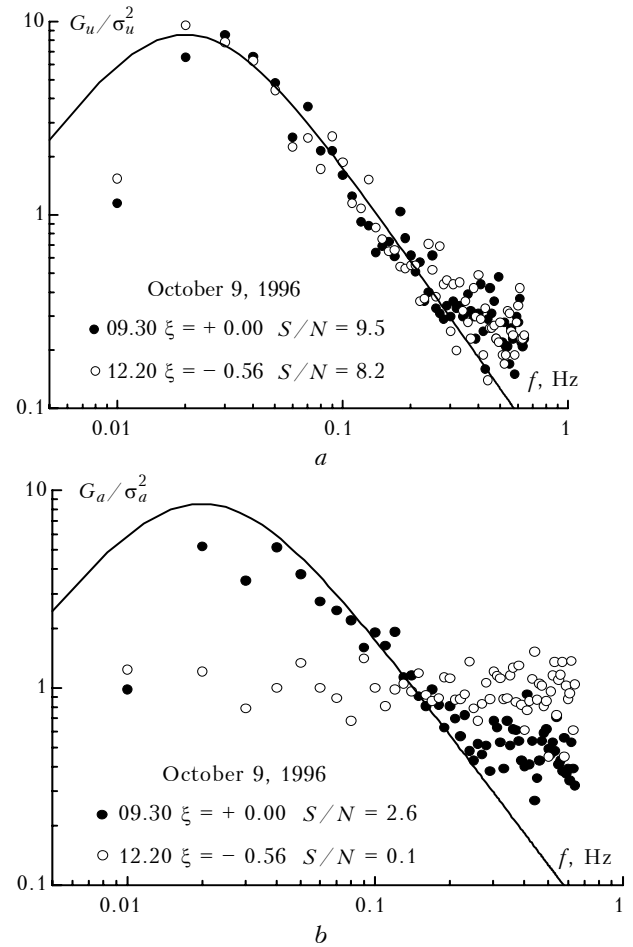


**Fig. 6.** Power spectra of fluctuations of longitudinal wind component (a) and aerosol (b) for  $\xi = 0$  (closed circles) and  $\xi = -0.56$  (open circles). Solid line shows the Kolmogorov's power law spectrum.

It is worth reminding that all observations have been done at only one altitude and, as such, they cannot be used to construct universal profiles of mean recorded parameters. Nevertheless, in Fig. 8 we plotted the normalized dimensionless values of mean velocity and scattering coefficient,  $\langle u \rangle / u_*$  and  $\langle A \rangle / A_*$ , versus parameter  $\xi$ , based on data collected in 1997. Formally, these values must be proportional to the corresponding universal functions; but due to the lack of data on additive constant (see formulas (22) and

(23), they show a scatter in Fig. 8. A closer look at the figure reveals a tendency for the data points to concentrate around some fitted curves, plotted by adjusting the coefficients for asymptotics of the universal functions and using the logarithmic plus linear model for stable conditions ( $\xi > 0$ ) and  $-1/3$  power law for the unstable ones ( $\xi < 0$ ).<sup>1</sup>

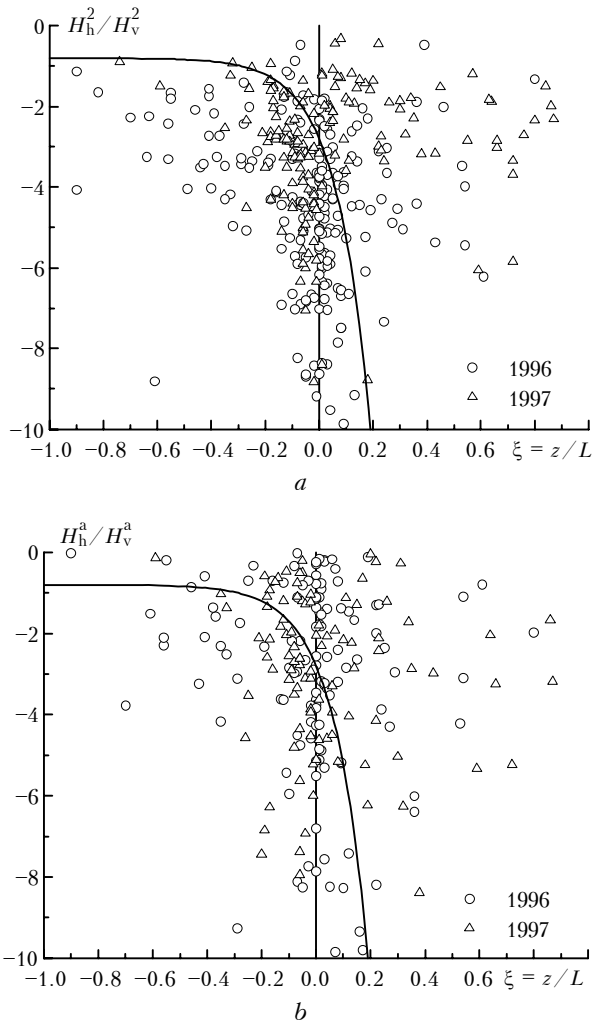


**Fig. 7.** Ratios of horizontal to vertical turbulent fluxes for heat (a) and aerosol (b) inferred from the measurement data obtained in 1996 and 1997.

Despite their preliminary and qualitative, rather than quantitative, character, the results presented in Fig. 8 demonstrate that the aerosol universal function for the mean value is remarkably similar in shape to analogous functions for velocity and temperature.

Aerosol is a complicated atmospheric constituent, usually calling for a complex approach for its study. So we suspect that a single parameter of hydrostatic stability may appear insufficient for an adequate treatment of the mean and random scattering properties. The point is that an increase in the atmospheric turbidity may be accompanied by changes in aerosol microphysics such as particle growth and

phase function deformation among others. To see what role does the turbulence play in these processes, or at least to formulate the problem more correctly, we have recorded continuous time series of measured meteorological parameters and scattering coefficients for the scattering angles of 45 and 170°. An additional intent was to explore how the scattering phase function changes with the hydrostatic stability parameter.

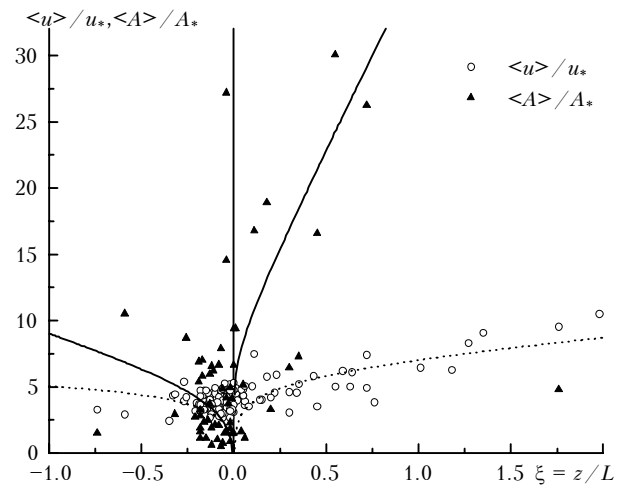


**Fig. 8.** Mean dimensionless values for wind velocity (circles) and aerosol (triangles) vs parameter  $\xi$  inferred from measurements in 1997.

The available data set was insufficient for making a summary, so we restricted our discussion to analysis of three days of continuous measurements, from June 30 to July 3, 1997.

The asymmetry parameter of the scattering phase function is defined as

$$A_\alpha = \langle \mu_{45} \rangle / \langle \mu_{70} \rangle, \quad (27)$$

where  $\mu$  is the scattering phase function at some scattering angle.

We will discuss briefly how nephelometer channels can be calibrated for scattering angles of 45 and 170°. Here this was done using a single-parameter regression model of scattering<sup>5</sup>:

$$\log \mu(\varphi) = K(\varphi) \log \sigma + \log C(\varphi), \quad (28)$$

where  $\sigma$  is the total scattering coefficient; and  $K(\varphi)$  and  $C(\varphi)$  are some empirical functions.

The formula for asymmetry parameter of the scattering phase function can be rewritten as

$$A_\alpha = \frac{\langle \mu_{45} \rangle}{\langle \mu_{70} \rangle} = \frac{C_{170} A_{45}}{C_{45} A_{170}}, \quad (29)$$

where  $C_{45}$  and  $C_{170}$  are calibration coefficients for nephelometer channels at scattering angles 45 and 170°. Using formulas (28) and (29), the ratio of calibration coefficients can be expressed as

$$\frac{C_{170}}{C_{45}} = \frac{\langle A_{170} \rangle}{\langle A_{45} \rangle} \times \times A_{\alpha} \sigma^{K(45)-K(170)} \times 10^{\log C(45)-\log C(170)}. \quad (30)$$

To evaluate (30), we use typical data<sup>5</sup> for Tomsk. Table 3 gives  $K(\varphi)$  and  $C(\varphi)$  values calculated for the scattering angles of 50 and 165°. The value of  $\sigma$  was set to 0.2 km<sup>-1</sup>, and that of  $A_{\alpha}$  to 4.2, as in Ref. 5.

Table 3

| $\varphi^{\circ}$ | $\log C(\varphi)$ | $K(\varphi)$ |
|-------------------|-------------------|--------------|
| 50                | -1.01             | 0.95         |
| 165               | -1.87             | 0.61         |

This calibration is used in Fig. 9 where the time series of measured parameters are shown. It is important that the atmospheric conditions gradually changed during experiment to clear-sky ones, from 9–10 cloud amount on June 29, 1997, to clear skies on July 3, 1997. Shown in Fig. 9a is the parameter of hydrostatic stability  $\xi$ , whose value is positive at night and negative during daytime, with the day-to-night variations progressively increasing in amplitude. The scattered signals at angles 45 and 170°, with calibration constant used, are shown in Fig. 9c. Corresponding signal variations  $V = (\sigma_A / \langle A \rangle) \times 100\%$  are given in Fig. 9d. The behavior of asymmetry factor  $A_{\alpha}$  of the scattering phase function is shown in Fig. 9b.

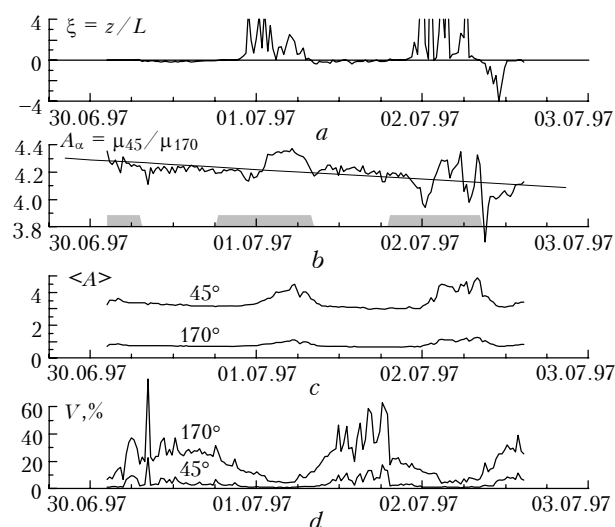


Fig. 9. Time series of the parameter  $\xi$  (a), asymmetry parameter of scattering phase function (b), scattered signals at angles 45 and 170° (c), and corresponding variation coefficients (d) inferred from the measurements in July 1997.

As seen, the scattering coefficients systematically decrease with time, together with  $A_{\alpha}$  value, a characteristic feature when total scattering coefficient decreases. During nighttime, at usually lower air temperatures and higher relative humidity, the scattering coefficients and, hence, parameter  $A_{\alpha}$  increased, the former by tens of a percent, and the latter by just a few

percent. Typically, the relative variance of fluctuations of the scattering coefficient decreased overnight and drastically increased by midday (Fig. 9d), in particular, due to a larger background noise illumination at this time. Normally, the correlation between measurements in different nephelometer channels was high approaching 0.8, on the average.

From Fig. 9 it follows that the shape of the scattering phase function was transformed only after the sign of atmospheric stratification changed from negative to positive. The scattering coefficients started to increase right after the establishment of stable stratification, whose duration is indicated with hatched bars in Fig. 9b. The “switch-off” of the mechanism of phase-function transformation is delayed in time, whereas its “switch-on” coincides with the time of the stratification sign reversal almost exactly.

## Conclusions

The analysis carried out here has shown that the open-cell nephelometer can be successfully used to study the pulsation in aerosol content due to turbulent air flow, except under strongly turbid conditions.

Observations made at IAO measurement site have revealed that the surface properties depend significantly on the dominating wind direction. They suggest that the observation conditions are most favorable when wind directions are from south to north or opposite, to within  $\pm 20^{\circ}$ .

Analysis of power spectra of fluctuations of scattering coefficient confirmed that, unless the signal-to-noise ratio is less than unity, the aerosol spectra are practically similar in shape to those of the wind velocity and the air temperature.

The obtained results, in terms of normalized dimensionless profiles of mean directional scattering coefficient, make us sure that the universal dependences for the mean and statistical properties of atmospheric aerosol, considered as a conservative passive admixture, can be obtained experimentally.

Studies of the statistical properties of the aerosol content pulsation must take aerosol microphysical properties into account.

## References

1. A.S. Monin, and A.M. Yaglom, *Statistical Hydrodynamics. Part 1* (Nauka, Moscow, 1965), 640 pp.
2. S.S. Zilitinkevich, *Dynamics of the Atmospheric Boundary Layer* (Gidrometeoizdat, Leningrad, 1970), 290 pp.
3. V.E. Zuev and G.M. Krekov, *Optical Models of the Atmosphere* (Gidrometeoizdat, Leningrad, 1986), 256 pp.
4. G.M. Krekov and R.F. Rakhimov, *Optical-Location Model of Continental Aerosol* (Nauka, Novosibirsk, 1982), 198 pp.
5. M.V. Kabanov, M.V. Panchenko, Yu.A. Pkhalagov, et al., *Optical Properties of Maritime Atmospheric Hazes* (Nauka, Novosibirsk, 1988), 201 pp.
6. G.I. Gorchakov and M.A. Sviridenkov, *Izv. Akad. Nauk, Fiz. Atmos. Okeana* **15**, No. 1, 53–59 (1979).

7. G.I. Barenblatt, *Applied Mathematics and Mechanics* **XVII**, No. 3, 261–274 (1953).
8. R. Otnes and L. Enokson, *Applied Analysis of Time Series* (Mir, Moscow, 1982), 428 pp.
9. S.P. Belyaev, N.K. Nikiforova, et al., *Optical-Electronic Methods of Aerosol Study* (Energoizdat, Moscow, 1981), 232 pp.
10. Yu.S. Balin, M.S. Belen'kii, et al., *Izv. Akad. Nauk, Fiz. Atmos. Okeana* **22**, No. 10, 1060–1063 (1986).
11. *Aerosols and their Climatic Effects*. Report of WMO (CAS) radiation commission of IAMAP Meeting of Experts. WCP-55, Williamsburg, 1983, 110 pp.
12. I.A. Rازenkov, A.P. Rostov, and N.A. Shefer, *Atmos. Oceanic Opt.* **6**, No. 10, 749–753 (1993).
13. Yu.S. Balin, M.S. Belen'kii, I.A. Rازenkov, A.P. Rostov, and N.V. Safronova, *Opt. Atm.* **1**, No. 8, 77–83 (1988).
14. I.A. Rازenkov, A.P. Rostov, and N.A. Shefer, *Atmos. Oceanic Opt.* **8**, No. 10, 820–826 (1995).
15. I.A. Rازenkov and A.P. Rostov, *Atmos. Oceanic Opt.* **10**, No. 7, 587–590 (1997).
16. G.Ya. Patrushev, A.P. Rostov, and A.P. Ivanov, *Atmos. Oceanic Opt.* **7**, Nos. 11–12, 890–891 (1994).
17. K.E. Kunkel, E.M. Eloranta, and J.A. Weinman, *J. Atmos. Sci.* **37**, No. 5, 978–985 (1980).
18. R.L. Kagan and L.S. Gandin, *Statistical Methods of Interpretation of Meteorological Data* (Gidrometeoizdat, Leningrad, 1976), 359 pp.